Condensed Matter Detonation: Theory and Practice

Craig M. Tarver

Lawrence Livermore National Laboratory, P. O. Box 808, Livermore, CA 94551, U.S.A.

INTRODUCTION

Detonations of high density, high energy solid and liquid organic explosives produce self-sustaining waves traveling at speeds approaching 10,000 m/s that reach approximately 40 GPa pressures and 4000 K temperatures in nanoseconds. These pressure-density-temperature states and short time durations are unique to detonation and thus are extremely difficult to study experimentally and theoretically. However, a great deal of progress has been made in understanding the hydrodynamics and chemistry that occurs with the reaction zone of a condensed phase detonation wave. This progress has been reviewed in several books [1-5] and bibliographies [6,7]. This chapter discusses significant progress over the past few years in two areas: the hydrodynamic theory of detonation and practical reactive flow modeling of detonation waves. The ultimate goal of condensed matter detonation research is to obtain an understanding of the underlying chemical and hydrodynamic phenomena equal to that of gas phase detonation. The current status of gas phase detonation theory and experimentation has been reviewed recently by Lee [8] and in several chapters of this book. The three-dimensional cellular structures of gas phase detonations have been carefully measured and can be accurately modeled using detailed chemical reaction rate models. Since gaseous detonation waves produce only approximately 20 times the initial gas pressures, they can be studied in shock tubes at universities. The perfect gas law can be used to describe the unreacted and reaction product equations of state. The kinetics of the individual chemical reactions can be measured individually by shocking mixtures of the species involved in each reaction of the decomposition process. The temperatures, particles velocities, densities, and pressures within the reaction zones can be measured and calculated. The equilibrium Chapman-Jouguet (C-J) state and the "hydrodynamic thickness" of a detonation wave can be measured. Concentration limits for detonation of many gaseous mixtures are known.

For condensed phase detonation waves, the three-dimensional cellular structure has been frequently observed indirectly [9], but has not yet completely quantified for pure liquid explosives or for solid explosives. The one-dimensional average reaction zone structures of many condensed phase explosives have been measured using embedded gauges [10], laser velocimetry techniques [11], and electrical conductivity probes [12] that average over the three-dimensional structure. These average states are modeled using

phenomenological, multidimensional reactive flow models [13]. The brightest temperatures at the C-J state of detonating transparent liquid and single crystal solid explosives have been measured by several groups [14] and can be calculated by chemical equilibrium computer codes, such as the CHEETAH code [15]. Many two-dimensional properties of condensed phase detonation waves, such as confined and unconfined failure diameter, wave front curvature, corner turning, divergence and convergence, metal acceleration ability, etc. have been experimentally measured and modeled [16]. Some three-dimensional experiments, for example the Los Alamos National Laboratory Prism Failure Test [17], have been developed and modeled [18]. Essentially, the overall "mechanical" aspects of condensed phase detonation (detonation velocity, von Neumann spike pressure, C-J pressure, reaction zone structure, reaction product equation of state, etc.) are well understood. However, the chemical aspects (chemical reaction rates, temperatures, species, etc.) are not well understood even for pure explosives. Since many explosives are mixtures, bonded with plastics, and/or contain aluminum or other metal particles, their chemical reaction rates are even more difficult to study. This chapter discusses the current state of the hydrodynamic theory of detonation and practical reactive flow modeling of condensed phase detonation and offers suggestions for future research.

CONDENSED PHASE DETONATION THEORY

One of the major developments in detonation theory in the last 30 years is the Non-Equilibrium Zeldovich - von Neumann - Doring (NEZND) theory. It was developed to identify the non-equilibrium chemical processes that precede and follow exothermic chemical energy release within the reaction zones of self-sustaining detonation waves in gaseous, liquid and solid explosives [19-25]. Prior to the development of the NEZND theory, the chemical energy released was merely treated as a heat of reaction in the conservation of energy equation in the Chapman-Jouguet (C-J) [26,27], Zeldovich - von Neumann - Doring (ZND) [28-30], and curved detonation wave front theories [31], and in hydrodynamic computer code reactive flow models [32]. NEZND theory has explained many experimentally observed detonation wave properties. These include: the induction time delays for the onset of chemical reaction; the rapid rates of the chain reactions that form the reaction product molecules; the de-excitation rates of the initially highly vibrationally excited products; the feedback mechanism that allows the chemical energy to sustain the leading shock wave front at an overall constant detonation velocity; and the establishment of the complex three-dimensional Mach stem structure of the leading shock wave fronts common to all detonation waves. When the leading shock front of a detonation wave compresses an explosive molecule, thermal energy must be transported into the vibrational modes of the explosive molecule before decomposition reactions can occur. The induction time for the onset of the initial endothermic reactions can be calculated using high pressure, high temperature transition state theory. The high-temperature, high-density calculations show the evolution of intermediate decomposition products and final stable detonation reaction products, such as H_2O, CO_2, N_2, CO and solid carbon. These reaction products are initially created in highly vibrationally excited

states that must be de-excited as chemical and thermal equilibrium are attained at the C-J state. Since the chemical energy is released well behind the leading shock front of a detonation wave, a physical mechanism is required for this chemical energy to reinforce the leading shock front and maintain its overall constant velocity. This mechanism is the amplification of pressure wavelets in the reaction zone by the process of de-excitation of the initially highly vibrationally excited reaction product molecules. The C-J state determines the energy delivery of the detonating explosive to its surroundings and thus must be accurately determined. Today's computers are still not large or fast enough to include all of these non-equilibrium processes in two- and three-dimensional hydrodynamic calculations of condensed phase detonation. Thus phenomenological high explosive reactive flow models are still being developed in various computer codes.

Figure 1 illustrates the various processes that occur in the NEZND model of detonation in condensed explosives. At the head of every detonation wave is a three-dimensional Mach stem shock wave front. There are several definitions of the width of a shock wave. Zeldovich and Raizer [33] defined shock wave width as the distance at which the viscosity and heat conduction become negligible. Behind each shock in the front, the phonon modes are first excited, followed by multi-phonon excitation of the lowest frequency vibrational (doorway) modes and then excitation of the higher frequency modes by multi-phonon up-pumping and internal vibrational energy redistribution (IVR) [34]. Internal energy equilibration is being studied in shocked liquid and solid explosives by Dlott et al. [35] and Fayer et al. [36]. Several first principle molecular dynamics studies of multi-phonon up-pumping and IVR plus the initial chemical reactions are being done at the atomistic scale [37]. After the explosive molecules become vibrationally excited, endothermic reactions can begin, followed by exothermic formation of stable products.

For gaseous explosives, the non-equilibrium processes that precede chemical reaction are easily measured, because they occur in nanosecond or longer time frames [33]. Velocities, pressures and temperatures are calculated using the perfect gas law. The high initial densities of liquids and solids make the measurement and calculation of the states attained behind a shock wave much more difficult, because the processes now take tens and hundreds of picoseconds and the perfect gas law does not apply. The distribution of the shock compression energy between the potential (cold compression) energy of the unreacted liquid or solid and its thermal energy is a complex function of shock strength.

The induction time for the initial endothermic bond breaking reaction can be calculated using the high pressure, high temperature transition state theory. Experimental unimolecular gas phase reaction rates under low temperature (<1000K) shock conditions obey the usual Arrhenius law:

$$K = Ae^{-E/RT} \tag{1}$$

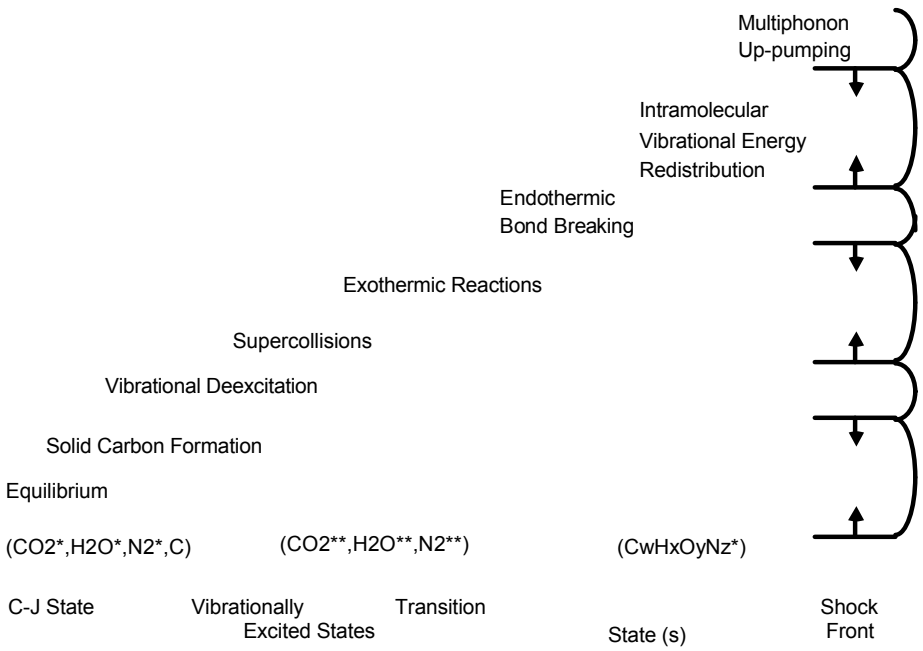

Figure 1. The Non-Equilibrium Zeldovich - von Neumann - Doring (NEZND) Theory of Detonation.

where K is the reaction rate constant, A is the frequency factor, E is the activation energy, R is the gas constant, and T is temperature. Current molecular dynamic and reactive force field potential calculations predict the onset of exothermic chemical in picoseconds immediately after the vibrational modes equilibrate [38]. However, subnanosecond time resolved laser interferometry experiments on detonating liquid and solid explosives have measured several nanosecond time delays for the exothermic reactions to begin at the average unreacted von Neumann spike conditions [11]. Nanosecond reaction zone measurements for solid explosives overdriven to pressures and temperatures exceeding those attained in self-sustaining detonation waves have shown that the reaction rates increase very slowly with shock temperature [39]. In kinetics terminology [40], the reaction rates "falloff" to slower rates than Eq. (1) predicts at high temperatures.

What causes this deviation from standard Arrhenius kinetic reaction rates at high temperatures and pressures? Eyring [41] attributed this "falloff" in unimolecular rates at the extreme temperature and density states attained in shock and detonation waves to the close proximity of vibrational states, which causes the high frequency mode that becomes the transition state for reaction to rapidly equilibrate with the neighboring modes by IVR. These modes form a "pool" of vibrational energy in which the energy required for decomposition is shared. Any large quantity of vibrational energy that a specific mode receives from an excitation process is shared among the modes before reaction can occur. Conversely, sufficient vibrational energy from the entire pool of oscillators is statistically present in the transition state vibrational mode long enough to cause reaction. When the

total energy in the vibrational modes equals the activation energy, the reaction rate constant K is:

$$K = (kT/h)e^{-s}\sum_{i=0}^{s-1}(E/RT)^{i}e^{-E/RT}/i! \qquad (2)$$

where k, h, and R are Boltzmann's, Planck's, and the gas constant, respectively, and s is the number of neighboring vibrational modes interacting with the transition state. The main effect of rapid IVR among s+1 modes at high densities and temperatures pressures is to decrease the rate constant dependence on temperature. Reaction rate constants have been calculated for detonating solids and liquids using Eq. (2) with realistic equations of state. Reaction rate constants from Eqs. (1) and (2) are compared to induction time results for liquid nitromethane, and single crystal pentaerythritol tetranitrate (PETN) in Figs. 2 and 3, respectively. Despite uncertainties in the calculated shock temperatures for various equations of state (EOS), it is clear that Eq. (2) agrees quite well with both sets of data using reasonable values of s. Extrapolations to the highest unreacted shock temperatures (approximately 2500K) within the three-dimensional structures of nitromethane and PETN detonation waves show that Eq. (2) predicts nanosecond reaction times in agreement with experiments, while Eq. (1) predicts picosecond reaction times. Thus Eyring's "starvation kinetics" or more precisely "high pressure, high temperature transition state theory" accurately calculates induction times for shock initiation and detonation of homogeneous liquid and heterogeneous solid explosives. After sufficient endothermic bond breaking has occurred, exothermic chain reaction processes dominate the detonation reaction zone.

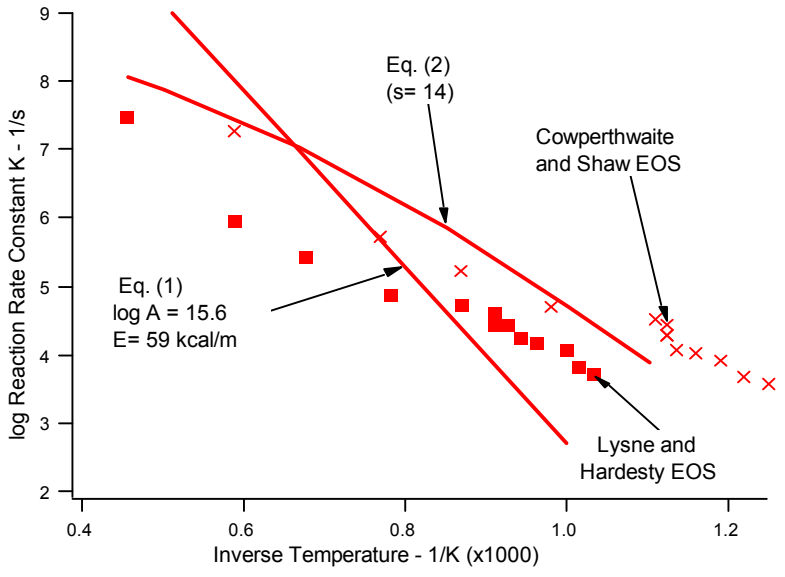

Figure 2. Reaction rate constants for nitromethane as functions of shock temperature

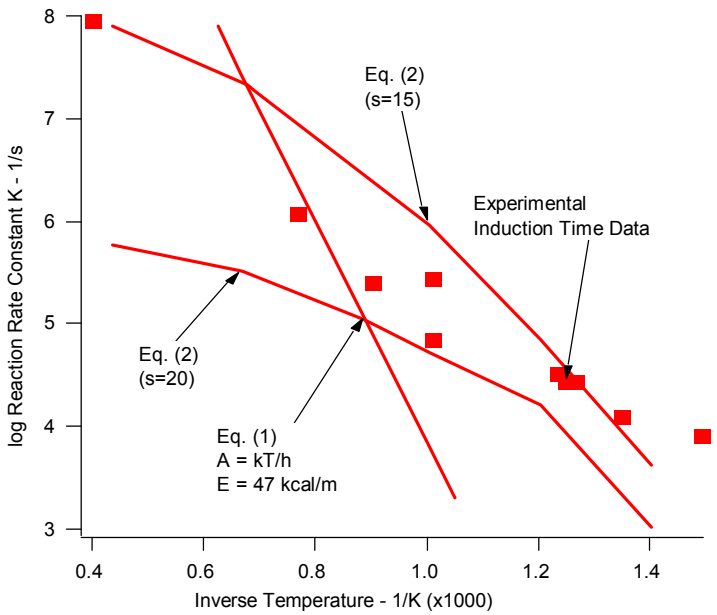

Figure 3. Reaction rate constants for single crystal PETN as functions of shock temperature

Following the induction and endothermic initial bond breaking processes, exothermic chain reaction processes follow in which reaction product gases (CO_2, N_2, H_2O, CO, etc.) are formed in highly vibrationally excited states [19-25]. These excited products either undergo reactive collisions with unreacted explosive molecules or non-reactive collisions with other products in which one or more quanta of vibrational energy is transferred. Some collisions are "super-collisions" [42] in which several quanta of vibrational energy are transferred. Since reaction rates increase rapidly with each quanta of vibrational energy available, reactive collisions dominate and the main chemical reactions are extremely fast. Once the chain reactions are completed, the remainder of the reaction zone is dominated by vibrational de-excitation of the gaseous molecules and carbon formation.

This vibrational de-excitation process controls the length of the reaction zone and provides the chemical energy necessary for shock wave amplification during self-sustaining detonation [22]. As pressure wavelets pass through the subsonic reaction zone, they are amplified by discrete frequency vibrational de-excitation processes. The opposite effect, shock wave damping by a non-equilibrium gas that lacks vibrational energy after expansion through a nozzle, is a well-known phenomenon [33]. These pressure wavelets then interact with the main shock front and replace the energy lost during compression, acceleration and heating of the explosive molecules. The pressure wavelet amplification process provides the chemical energy required to develop a complex, three-dimensional Mach stem shock front structure, as shown in Fig. 1. This structure has been observed for gaseous, liquid and solid explosives [43] and is currently being replicated for gaseous explosives in two-dimensional and three-dimensional hydrodynamic computer simulations

using multiple reaction chemical kinetic schemes [44]. Simulations using reduced kinetic schemes for condensed phase detonation are also being attempted [45].

Since most condensed phase explosive formulations are under-oxidized, significant amounts of solid carbon particles form in the chemical reaction zone of self-sustaining detonation waves. These particles are diamond, graphite, or amorphous carbon depending on the temperatures and pressures attained in the reaction zone and have diameters of about 10 nanometers independent of the amount of explosive detonated [46]. Since the solid carbon formation process is diffusion controlled as carbon atoms attempt to form chains and particles in the presence of several gaseous species, this process requires more time than gaseous product formation and thermal equilibration. Thus the chemical energy release portion of a condensed phase detonation wave exhibits two energy release rates: a fast reaction taking tens of nanoseconds in which the main gaseous products form and equilibrate followed by a slower reaction for the solid carbon particle formation requiring hundreds of nanoseconds. These rates have been measured by several nanosecond time resolved techniques including: embedded particle velocity and pressure gauges, electrical conductivity probes; and laser interferometry [47]. Chemical and thermal equilibrium at the C-J state is closely approached after the nanometer size carbon particles form. A rarefaction wave in which the products expand and cool follows the detonation reaction zone. This expansion process does the useful work on surrounding materials. The C-J state and subsequent expansion can be measured by metal acceleration experiments [48] and calculated using modern thermochemical equilibrium computer codes, such as the CHEETAH code [15].

Detonation reaction zones can be more complex for mixtures of explosive materials and for formulations containing metals that react with the product gases. Aluminum particles are added to organic explosives to provide later-time (microsecond to millisecond) energy release when the gaseous products CO_2, CO and H_2O penetrate the aluminum oxide outer layer and react with molten aluminum to form Al_2O_3 and various aluminum suboxides (AlO, Al_2O, AlO_2, etc.). Under various conditions, aluminum oxidation liberates its large amount of thermal energy on different time scales [49]. Aluminum particles that do not react with the detonation products may react with oxygen from air, if the cloud of detonation products turbulently mixes with air behind the blast wave [50,51].

Even with today's large, fast multiprocessor computers, all of the aforementioned chemical processes can not be included in practical one-, two-, and three-dimensional hydrodynamic code calculations of initiation and propagation of condensed phase detonations in large explosive charges. Unlike gaseous detonations, the temperatures and species concentrations cannot yet be measured or calculated in the reaction zones of detonating solid and liquid explosives. Therefore practical, phenomenological reactive flow models of detonation, such as the Ignition and Growth model [32], have been developed to calculate the main features of shock initiation and detonation reaction zones and subsequent metal acceleration during reaction product expansion. The practical application of the Ignition and Growth model to insensitive high explosives based on the triaminotrinitrobenzene (TATB) molecule is discussed in the next section.

PRACTICAL MODELLING OF DETONATION: IGNITION AND GROWTH

All chemical reaction rates are governed by the local temperature of the molecules that are about to react. However, since temperatures in detonating condensed phase explosives have not been measured, phenomenological reactive flow models using rate laws based on properties that can be measured, such as pressure and compression, are currently used to model condensed phase shock initiation and detonation. All of these reactive flow models require as a minimum: two equations of state, one for the unreacted explosive and one for its reaction products; a reaction rate law for the conversion of explosive to products; and a mixture rule to calculate partially reacted states in which both explosive and products are present. The most widely used model is the Ignition and Growth reactive flow model, [32] which uses two Jones-Wilkins-Lee (JWL) equations of state, one for the unreacted explosive and another one for the reaction products, in the temperature dependent form:

$$p = A\, e^{-R_1 V} + B\, e^{-R_2 V} + \omega C_V T/V \qquad (3)$$

where p is pressure in Megabars, V is relative volume, T is temperature, ω is the Gruneisen coefficient, C_V is the average heat capacity, and A, B, R_1, and R_2 are constants. The unreacted explosive equation of state is fitted to the available shock Hugoniot data, and the reaction product equation of state is fitted to cylinder test and other metal acceleration data. At the high pressures involved in shock initiation and detonation of solid and liquid explosives, the pressures of the two phases must be equilibrated, because collisions between the hot gases and the explosive molecules at hundreds of kilobars pressure occur on subnanosecond time scales based on the sound velocities of the components. Various assumptions have been made about the temperatures in the explosive mixture, because heat transfer from the hot products to the cooler explosive is slower than the pressure equilibration process. In this version of the Ignition and Growth model, the temperatures of the unreacted explosive and its reaction products are equilibrated. Temperature equilibration is used, because heat transfer becomes increasingly efficient as the reacting "hot spots" grow and consume more explosive particles as the high pressures and temperatures associated with detonation are approached. Fine enough zoning must be used in all reactive flow calculations so that the results have converged to answers that do not change with finer zoning. Generally this requires a resolution of at least 10 zones for the detonation reaction zone. The insensitive solid explosive LX-17 (92.5% triaminotrinitrobenzene (TATB) and 7.5% Kel-F binder) has an experimentally measured reaction zone length of three mm [52] so using 10 zones per mm spreads the reaction over 30 zones and results in converged calculations.

The Ignition and Growth reaction rate equation is given by:

$$dF/dt = I(1-F)^b(\rho/\rho_o - 1 - a)^x + G_1(1-F)^c F^d p^y + G_2(1-F)^e F^g p^z \qquad (4)$$

$$0<F<F_{igmax} \qquad 0<F<F_{G1max} \qquad F_{G2min}<F<1$$

where F is the fraction reacted, t is time in μs, ρ is the current density in g/cm^3, ρ_o is the initial density, p is pressure in Mbars, and I, G_1, G_2, a, b, c, d, e, g, x, y, z, F_{igmax}, F_{G1max}, and F_{G2min} are constants. This three-term reaction rate law represents the three stages of reaction generally observed during shock initiation and detonation of pressed solid explosives [32]. The first stage of reaction is the formation and ignition of "hot spots" caused by various possible mechanisms (void collapse, friction, shear, etc.) as the initial shock or compression wave interacts with the unreacted explosive. The fraction of solid explosive heated to high temperatures in "hot spots" during shock compression is approximately equal to the original void volume. For shock initiation modeling, the second term in Eq. (4) then describes the relatively slow process of the inward and/or outward growth of the isolated "hot spots" in a deflagration-type process. The third term represents the rapid completion of reaction as the "hot spots" coalesce at high pressures and temperatures, resulting in a fast transition from shock induced reaction to detonation.

For detonation modeling, the first term also reacts a quantity of explosive less than or equal to the void volume after the explosive is compressed to the unreacted von Neumann spike state. The second term in Eq. (2) models the fast decomposition of the solid into stable reaction product gases (CO_2, H_2O, N_2, CO, etc.). The third term describes the relatively slow diffusion limited formation of solid carbon (amorphous, diamond, or graphite) as the chemical and thermodynamic equilibrium C-J state is approached. Experimentally, only nanometer size solid carbon particles are recovered after detonation of even very large explosive charges [53]. This implies that the growth of the carbon particles stops at the high pressures and temperatures associated with the C-J state. These reaction zone stages have been observed experimentally using embedded gauges, laser interferometry, and electrical conductivity probes [54-56].

The Ignition and Growth reactive flow model has been applied to a great deal of experimental data using several one-, two-, and three-dimensional hydrodynamic codes. For shock initiation, it has successfully calculated embedded gauge, run distance to detonation, short pulse duration, multiple shock, reflected shock, ramp wave compression, gap tests, and divergent flow experiments on many high explosives at various initial porosities and temperatures [57-59]. For detonation, the model has successfully calculated embedded gauge, laser interferometric metal acceleration, failure diameter, corner turning, converging, diverging, and overdriven experiments [60-63]. Examples of one-, two- and three-dimensional applications are shown for the TATB-based explosives LX-17 (92.5% TATB and 7.5% Kel-F binder) and PBX 9502 (95% TATB and 5% Kel-F).

Two one-dimensional nanosecond time resolved experimental records and Ignition and Growth calculations are shown in Figs. 4 and 5. Figure 4 shows the measured and calculated interface velocity histories for detonating LX-17 impacting various salt crystals [13]. The von Neumann spike state, a relatively fast reaction, a slower reaction, and finally the initial expansion of the products are clearly evident in Fig. 4. Figure 5 illustrates the measured and calculated free surface velocities of a 0.267 mm thick tantalum disc driven by 19.871 mm of detonating LX-17 [13]. The momentum associated with the LX-17 reaction zone and early product expansion are accurately measured and calculated. These and other one-dimensional experiments were used to calibrate the LX-

17 and PBX 9502 Ignition and Growth reaction rate parameters, which are then tested against two- and three-dimensional experimental data from several laboratories.

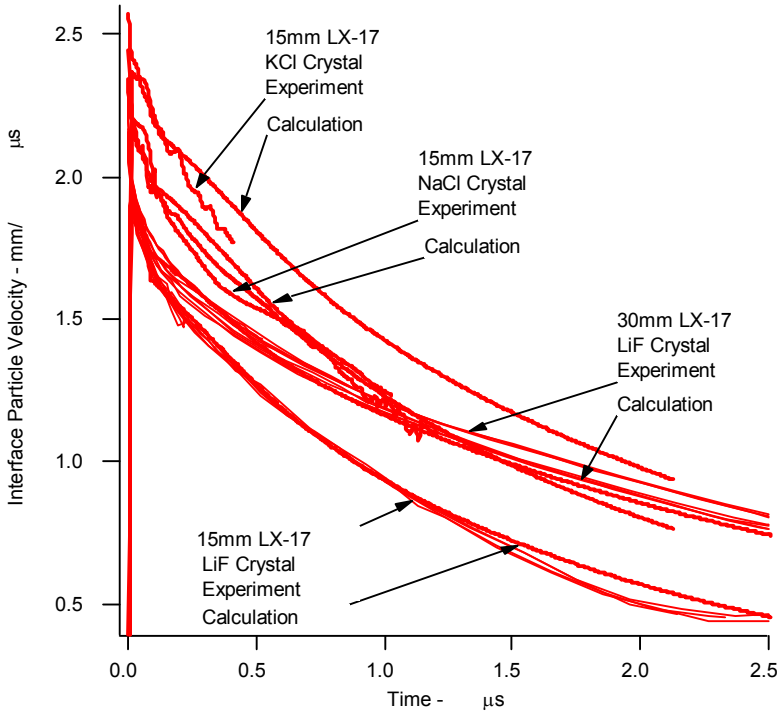

Figure 4. Interface particle velocity histories for detonating LX-17 and salt crystals

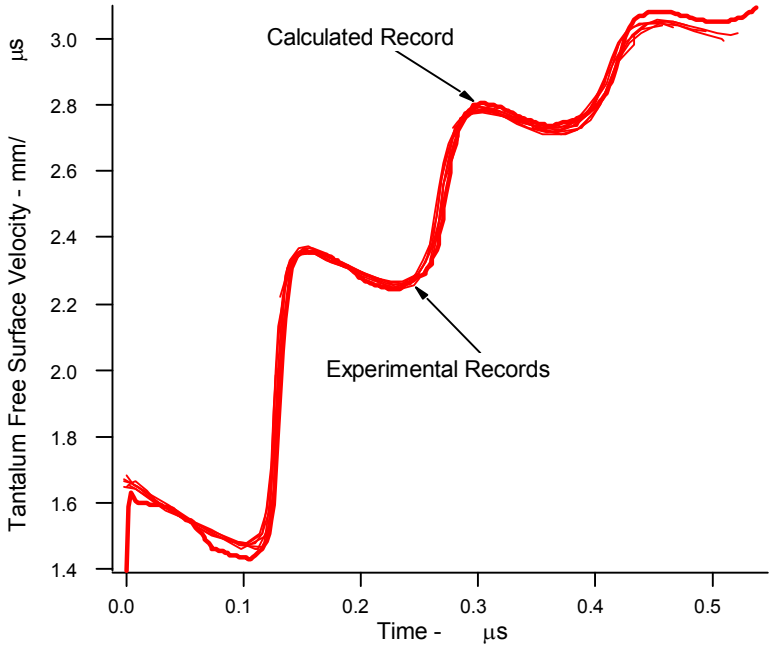

Figure 5. Free surface velocity of a 0.267 mm thick tantalum disk driven by 19.871 mm of LX-17

The main two-dimensional detonation experiment at LLNL is the cylinder expansion performance test [16]. Figure 6a shows the radial velocity histories for a 2.54 cm radius LX-17 charge confined by 0.272 cm of copper. To accurately calculate the momentum imparted to the cylinder wall, the Ignition and Growth model plus the Steinberg-Guinan or Johnson-Cook metal model must be used. In a certain range of LX-17 to copper thickness ratios, the copper wall can spall and the resulting wall acceleration profile is not as regular. Figure 6b shows the experimental and calculated radial wall velocities for the case of copper spall calculated using a spall model with the Steinberg-Guinan model [16].

Another example of unique two-dimensional TATB detonation wave structure is shown in Fig. 7 in which EDC35 (95% TATB and 5% Kel-F) is sandwiched between brass (left

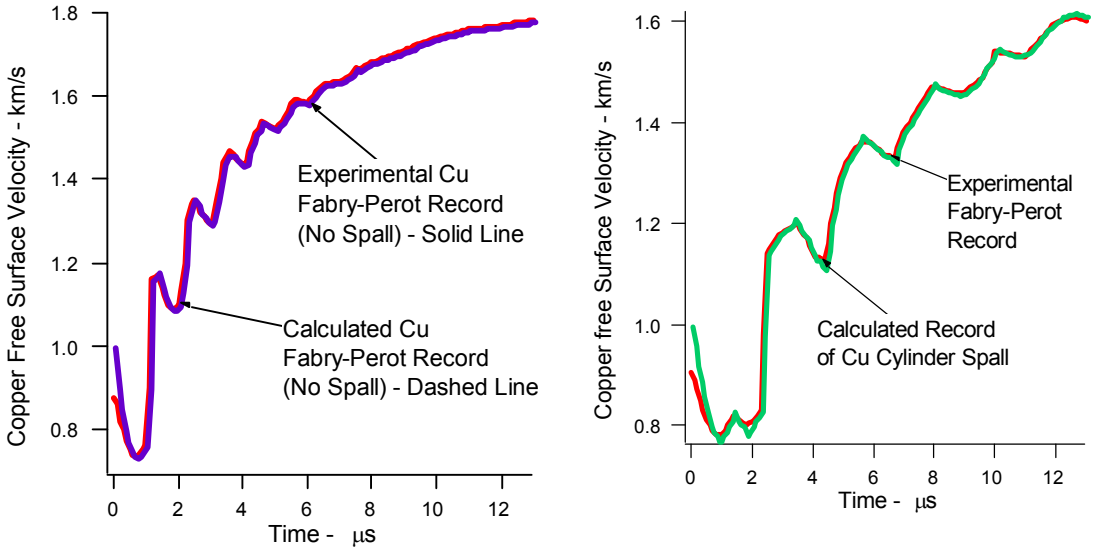

Figure 6. Experimental and calculated LX-17 copper cylinder test radial free surface velocities

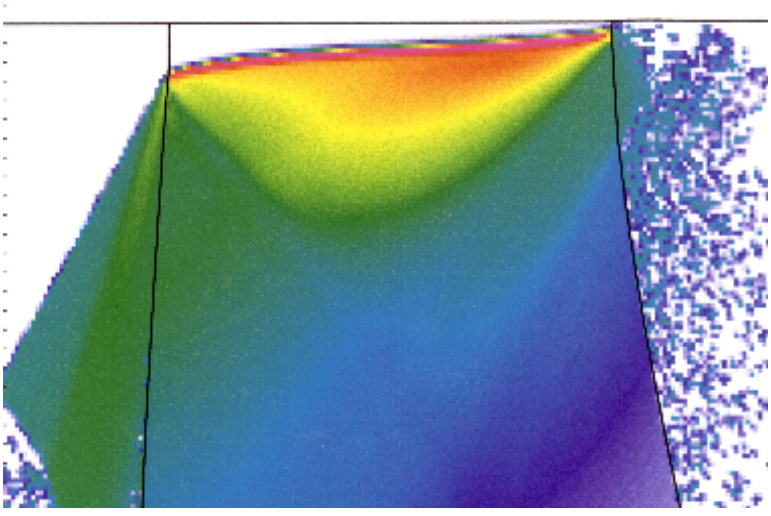

Figure 7. LX-17 detonation wave propagating between brass (left side) and beryllium (right side)

side) and beryllium (right side) [16]. Brass, like most metals, has a lower shock velocity than the detonation velocity of EDC35, so the brass shock front lags behind the detonation wave. Beryllium has a higher shock velocity than the EDC35 detonation velocity, and thus its shock wave pulls the detonation wave along at higher velocity than its C-J value. The curved shape of the EDC35 detonation wave and the arrival times of the wave at both edges after various propagation lengths are accurately calculated by the Ignition and Growth model parameters for PBX 9502. [16]

The detonation wave front curvature is often measured as the detonation wave reaches the surface of an unconfined or confined cylindrical explosive charge. This wave curvature and the associated decrease in detonation velocity for a finite diameter charge is the result of the interaction of the chemical reaction rates with the radial rarefaction wave that propagates from the outer explosive boundary and reduces the pressure, temperature, and reaction rates in the reaction zone [64]. Since TATB has very high activation energies for its decomposition reactions, its plastic bonded explosives (PBXs) like LX-17 fail to detonate at velocities below 96 - 97% of the C-J detonation velocity [64]. This is similar to pure liquid explosives such as nitromethane, which also have high activation energies for decomposition [64]. The measured and calculated detonation wave front curvatures for confined LX-17 by copper, PMMA and tantalum (calculation only) are shown in Fig. 7 [16]. Most other solid explosives exhibit larger detonation velocity decreases with decreasing charge diameter before failing to detonate [25,64,65].

Since TATB-based detonation waves are very sensitive to rarefaction waves, they have strong interactions with changes in geometry and exhibit regions of zero or partial reaction in spherical divergence [66] or corner turning [67,68] experiments. To insure correct wave propagation and impulse delivery when modelling complex geometries that cannot be tested, reactive flow models must closely simulate these two-dimensional experiments.

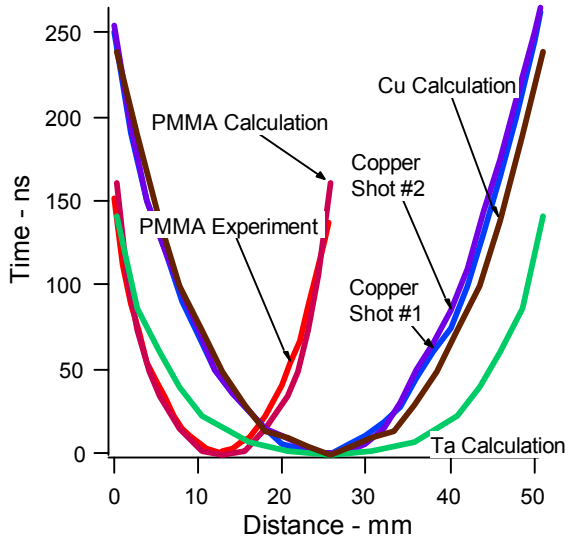

Figure 7. LX-17 detonation wave front curvature for copper, PMMA and tantalum cylinders

One well instrumented corner turning experiment is the "Hockey puck" experiment shown in Fig. 8 [69]. A 19.05 mm radius hemispherical booster of Ultrafine (UF) TATB, which is fine particle TATB pressed to 1.8 g/cm^3, is initiated at the center of the hemisphere. A spherically divergent detonation wave is established which initiates the LX-17 charge. The LX-17 detonates spherically outward, but also attempts to turn the corner and detonate the LX-17 in the region from 0 to 15 mm in Fig. 8. As it turns the corner, the LX-17 detonation wave leaves a region of unreacted or partially reacted explosive near the corner. These "dead zone" regions have been observed using X-rays [67,69] and proton radiography [68]. The "Hockey Puck" experiments also measured the times of arrival of the LX-17 detonations at various positions along their perimeters. The experimental and calculated times of arrival for the LX-17 detonation wave in a 12.7 mm wide "Hockey Puck" experiment are shown in Fig. 9. Excellent agreement is obtained using previously determined LX-17 Ignition and Growth parameters. Additional "Hockey Pucks" have since been fired using different widths of LX-17, PBX 9502 as the acceptor charge, and LX-07 (90% HMX and 10% Viton binder) as the booster explosive [18,70].

Besides turning 90˚ corners, detonation waves are propagated around 90˚ and 180˚ arcs of various inner and outer radii with unconfined or confined boundaries. Unconfined LX-17 90˚ arc tests fired by Lyle and Hayes were modeled by Tarver and Chidester [71]. Lyle's arc had an inner radius of 8.89 cm and an outer radius of 11.43 cm, while Hayes' arc had a 6.35 cm inner radius and a 10.16 cm outer radius. Figure 10 shows the experimental and calculated wave velocities at various angles along the outer edge of Lyle's arc. The average calculated phase velocity from 0˚ to 90˚ is 8.781 km/s, while the measured value is 8.667 km/s for 0˚ to 85˚. The inner surface pins measured a constant velocity of 7.289 km/s from 0˚ to 84˚, while the calculated inner surface velocity equaled

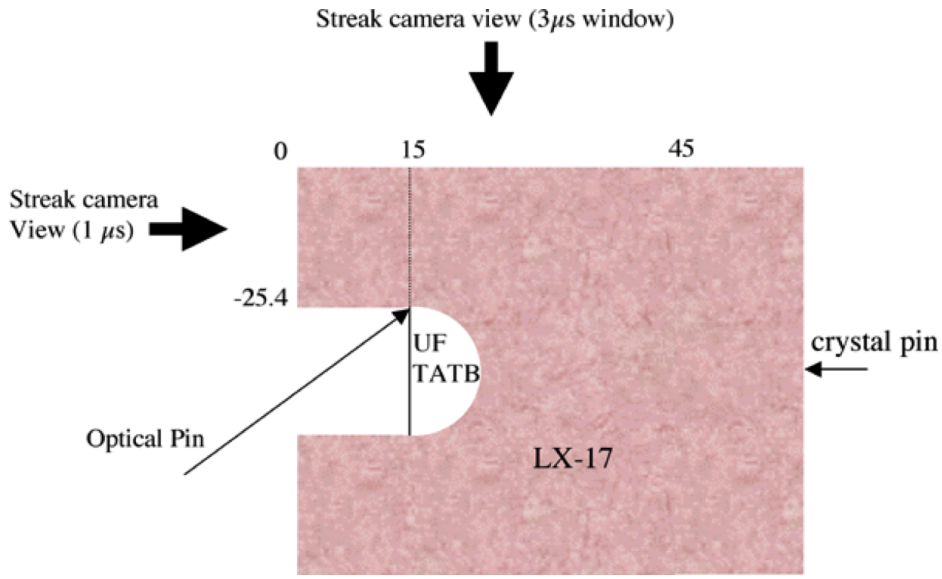

Figure 8. Experimental geometry for a 25.4 mm wide LX-17 "Hockey Puck"

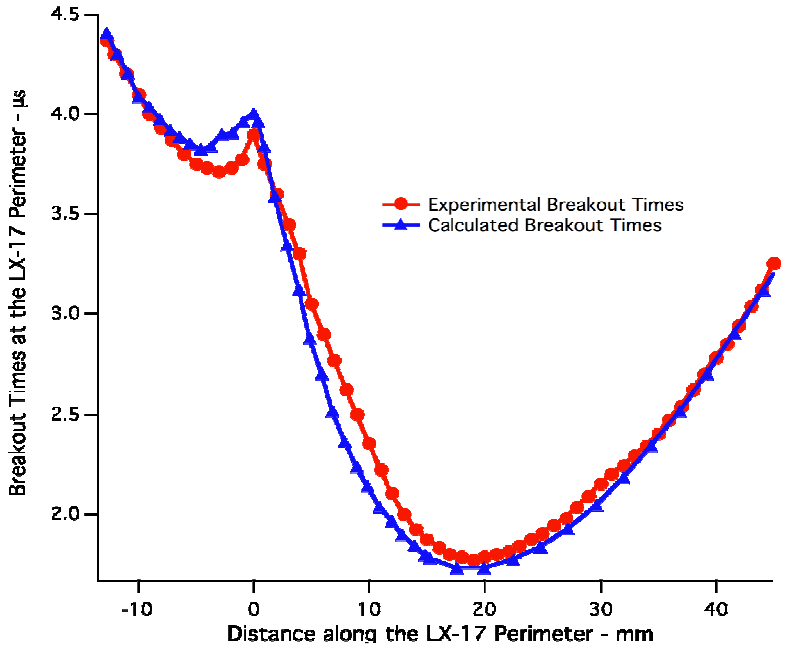

Figure 9. Experimental and calculated breakout times along the LX-17 perimeter for a 12.7 mm wide "Hockey Puck"

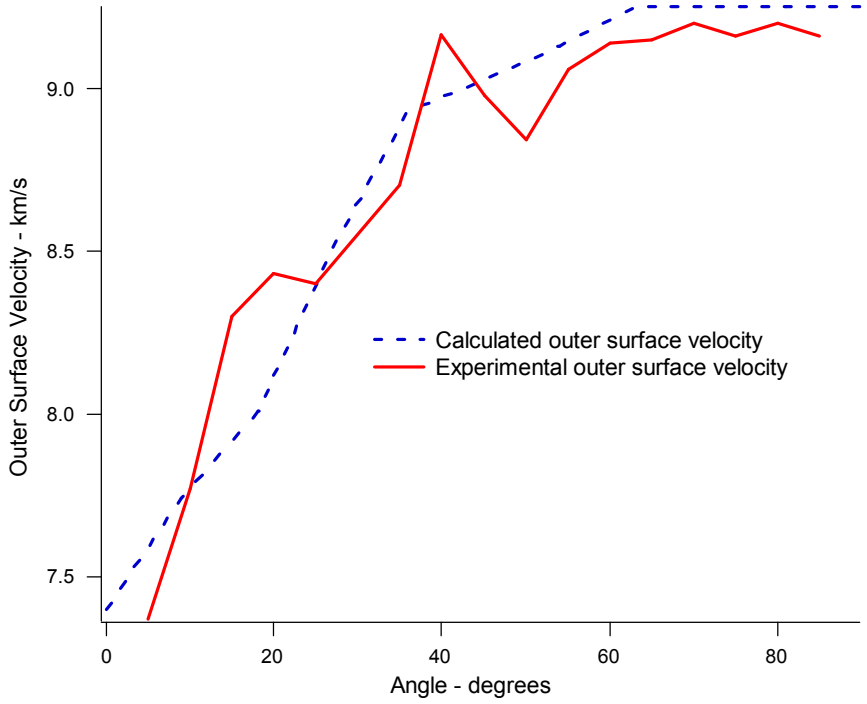

Figure 10. Experimental and calculated outer surface velocities versus angle for the Lyle arc

7.241 km/s. For the Hayes' arc, the measured inner edge velocity was 7.03 km/s, while the calculated value was 7.042 km/s. The measured outer surface velocity was 10.07 km/s,

and the calculated value was 9.75 km/s. Both the experimental and calculated initial wave breakouts were 3 mm from the inner edge.

A set of confined TATB arc experiments was published by Lubyatinsky et al. [71] and modeled by Tarver and Chidester [70]. These experiments used 180˚ TATB explosive arcs with outer radii of 6 cm and inner radii of 3, 4 and 5 cm confined on both edges by 1 cm of steel or PMMA. Time of arrival pins were placed every 15˚ degrees along both explosive edges. The edge wave velocities measured for the 180˚ arcs were slightly less than those calculated by the LX-17 model. Figure 11 contains the experimental and calculated arrival time differences for the three LX-17 thicknesses with steel confinement, while Fig. 12 shows the arrival time differences for PMMA confinement. The calculated and experimental arrival time differences agree closely for the steel confined charges, while the calculated differences are larger than those measured for the 20 mm and 30 mm thick arcs confined by PMMA. The experiment and the simulation show failure of the 10 mm thick TATB arc confined by PMMA after about 90˚ of travel.

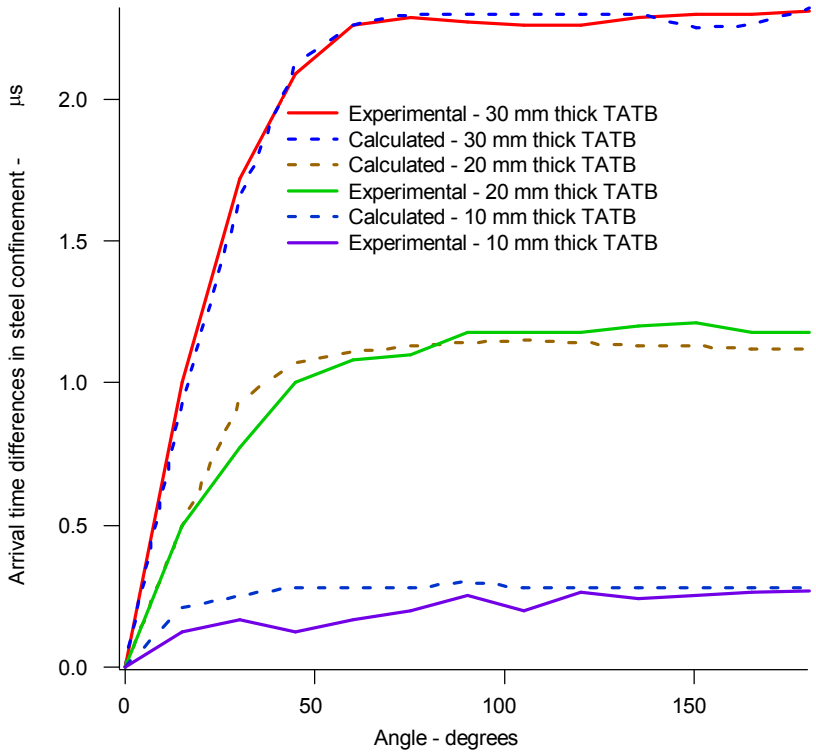

Figure 11. Arrival time differences in steel confinement versus angle for three thicknesses of TATB arcs

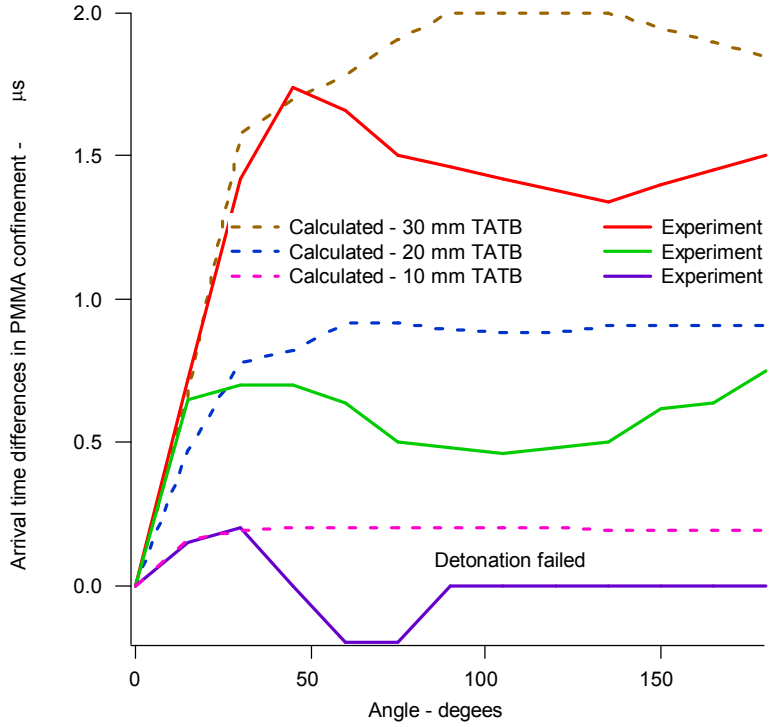

Figure 12. Arrival time differences in PMMA confinement versus angle for three TATB thicknesses

The final two-dimensional detonation wave propagation comparison of the LX-17/PBX 9502 Ignition and Growth model with experiments is for the cones of various areas reported by Salyer and Hill [72]. They reported the edge detonation velocities as functions of inverse radius of PBX 9502 cones with included angles of 10˚, 20˚, 30˚, 40˚, 80˚ and 90˚. As the steady PBX 9502 waves enter the converging cones, they are overdriven to higher velocities and shock pressures and temperatures than the Chapman-Jouguet (C-J) and von Neumann spike values [11]. At 40˚, 80˚ and 90˚, the converging detonation waves propagate through the entire cones at greater than C-J velocities. At 10˚, 20˚ and 30˚, the convergence effects are overcome by rarefaction waves, which reduce the reaction rates until they separate from the shock fronts. Then the detonation waves immediately fail. To simulate these effects, the 2D conical tests were calculated using 20 zones per mm and the PBX 9502 parameters. Figure 13 shows the experimental and calculated edge velocities as functions of inverse cone radius for the 40˚, 80˚ and 90˚ cones, along with the unconfined detonation velocity-inverse radius curve [6]. The calculated detonation waves detonated to the tips of the cones. The 80˚ and 90˚ cones remained overdriven at edge velocities exceeding 10 km/s. Figure 14 shows the 10˚, 20˚ and 30˚ comparisons. These calculated detonation waves failed to detonate to the tips of the cones. The calculated failures occurred at a slightly larger radius than the 30˚ cone test and at slightly smaller radii than the 10˚ and 20˚ cone tests. The overall agreement is excellent for detonation waves that are initially highly overdriven and then fail rapidly.

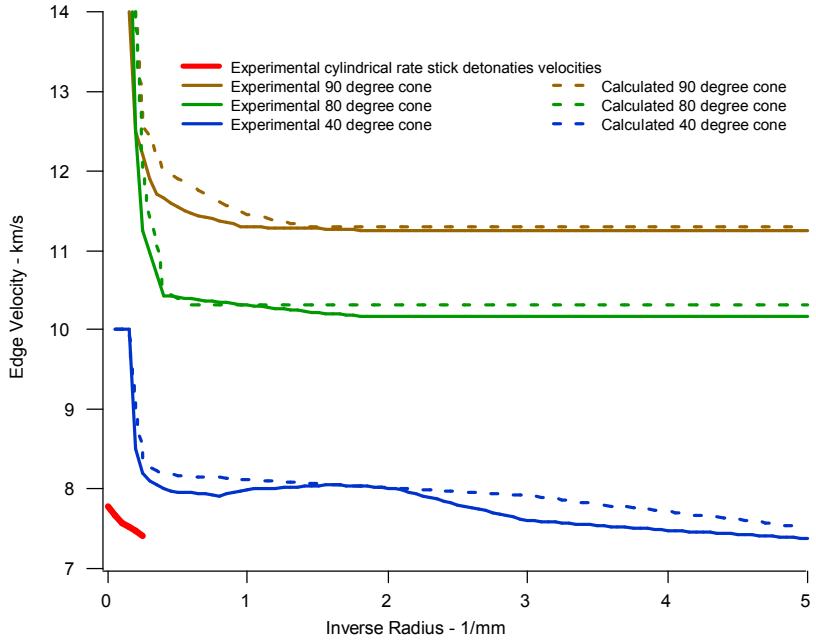

Figure 13. Experimental and calculated edge velocities for the 40˚, 80˚ and 90˚ cones

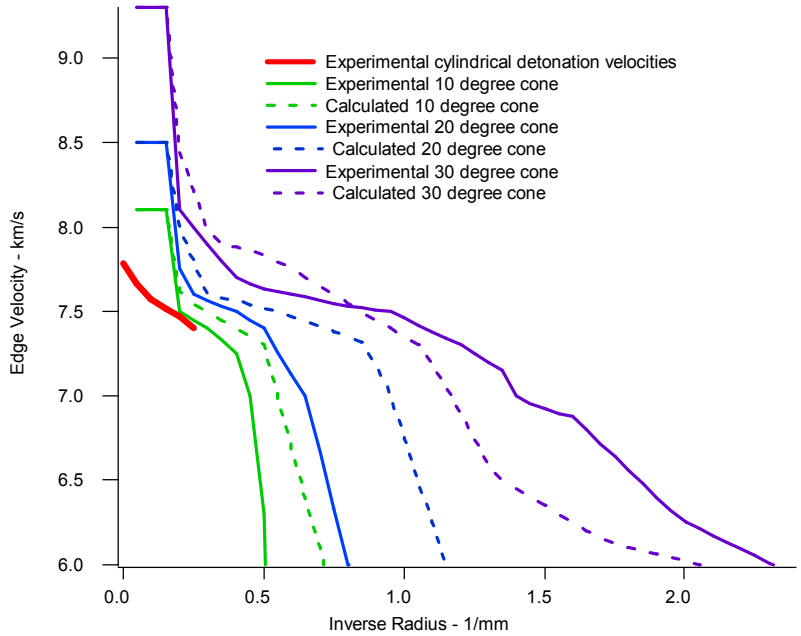

Figure 14. Experimental and calculated edges velocities for the 10˚, 20˚ and 30˚ cones

One other fascinating detonation phenomena for which two-dimensional experimental data was recently obtained is "shock desensitization." This phenomenon was previously known as "dead pressing" and has been observed in several explosives, including very sensitive primary explosives [73]. In the first quantitative study of shock desensitization, Campbell and Travis [74] impacted large PBX 9404 (94% HMX, 3% nitrocellulose, and 3% chloroethylphosphate) and Composition B (65% RDX/35% TNT) charges with weak shocks on one edge and initiated detonations on another edge. They then measured the interactions of these detonation waves with weak shocks of various strengths. For a certain shock pressure regime (1 – 2.4 GPa) in both PBX 9404 and Composition B, the detonation waves propagated a few millimeters into the pre-compressed explosive and then failed abruptly. The measured time duration before failure was close to the experimental measured shock initiation time for that specific shock pressure. For shock pressures below 1 GPa, which did not pre-compress the unreacted explosives to their maximum densities, the detonation waves wavered slightly but continued to detonate through the pre-compressed explosive that still contained some hot spot reaction sites. At shock pressures greater than 2.4 GPa, the detonation waves encountered compressed explosives with growing hot spots so they continued to detonate through the compressed, reacting explosives.

Recently, five new experiments were designed to pre-compress LX-17 in the 1 - 2 GPa pressure range by diverging shocks propagating through steel shadow plates, while the LX-17 detonation waves are propagating around two corners [75,76]. The LX-17 detonation waves then arrive in weakly shocked regions of pre-compressed LX-17. If the diverging shock pressures are high enough and are applied long enough, the pre-shocked LX-17 becomes shock desensitized and the detonation waves fail. If the shocks are not strong enough or too strong, the detonation waves continue to detonate. Based on input parameters estimated from the higher pressure, Hockey Puck dead zone experiments, the Ignition and Growth model including shock desensitization predicted that desensitization would occur in all five experiments.

Figure 15 is a cross section of one of the double corner turning and shock desensitization experiments. Under the stainless steel shadow plate, a small charge of the PETN based explosive LX-16 initiates detonation of a UF TATB hemispherical booster. The UF TATB is pressed to 1.80 g/cm^3 or 93% theoretical maximum density. The main LX-17 charge surrounds the UF TATB booster. On the top and bottom are the 6 mm thick aluminium witness plates. Upon firing, the small LX-16 explosive charge initiate the hemispherical UF TATB booster, which in turn initiates a LX-17 hemispherical detonation. The LX-17 detonation propagates outward until it reaches the aluminium plates. The bottom aluminium plate contains three time-of-arrival pins to check that a diverging LX-17 detonation was initiated. The top aluminium plate is instrumented with eight photonic Doppler velocimetry (PDV) probes to measure the free surface velocity at eight radii. X-ray radiographs and framing camera images are taken at various times. The LX-17 detonation propagates around the two corners of the steel shadow plates and into a thin LX-17 region between the steel shadow plate and the top aluminium plate.

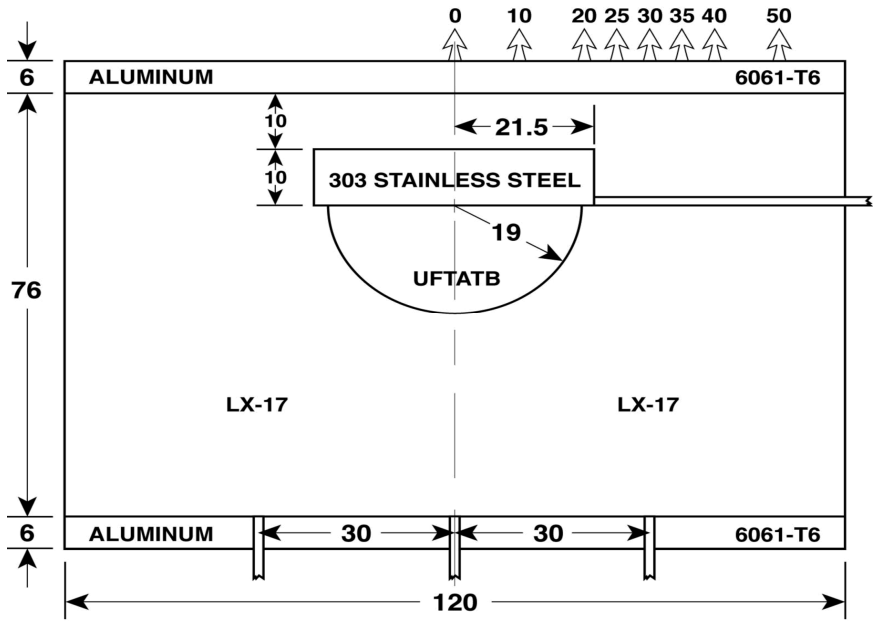

Figure 15. Cross section of a double corner turning and shock desensitization test (in mm)

These LX-17 regions are compressed to 1 to 2 GPa by diverging shock waves that had propagated through the steel shadow plates. These weak shocks desensitize LX-17, resulting in failures of LX-17 detonation waves when they reached these LX-17 regions.

To model shock desensitization in doubly shocked LX-17, a second compression constant was added to the first term of the reaction rate law in Eq. (2) by Tarver et al. [77]. This forced that the reaction rate to be zero when the LX-17 was shocked within a range of compressions. This assumption worked well for LX-17 shock desensitization due to reflected shocks. However, it has been shown that shock desensitization is time dependent [74]. The failure of detonation in the pre-compressed explosive requires approximately the same time as shock initiation at that shock pressure. For TATB PBX's, it has been shown using proton radiography that dead zones can exist for relatively long times after detonation waves turn corners [67]. The regular Ignition and Growth model creates dead zones and propagates around one corner extremely accurately, but allows the partially reacted dead zone regions to slowly react at late times [69]. To model these longer lasting dead zones, a time dependent desensitization rate law was added to the Ignition reaction rate term in Eq. (4) by DeOliveira et al. [78] The desensitization rate S is defined as:

$$S = Ap(1 - f)^{\varepsilon} \qquad (5)$$

where A is a constant, p is the shock pressure, ε is a small constant, and f varies from zero in a pristine explosive to one in a fully desensitized explosive. The density threshold a in Eq. (4) is redefined to be a linear function of f:

$$\underline{a}\underline{f} = \underline{\tilde{a}}_1 \underline{f} a_1 \underline{f} \qquad (6)$$

where a_0 and a_1 are constants. The relative density threshold for ignition of the pristine explosive becomes $1 + a_0$, and, for the fully desensitized explosive, the relative density for ignition becomes $1 + a_1$. Additionally, the second reaction rate term in Eq. (4) is modified so that it turns on only when F exceeds a minimum F_{G1min}, which is a linear function of f:

$$F_{G1min}(f) = F_c f \qquad (5)$$

where F_c is a constant related to the initial porosity. This second modification provides a competition between desensitization and reaction growth and thus determines an extinction mechanism. This modification introduces four new parameters: A, ε, a_1, and F_c. No well defined, time resolved experiments, such as those of Campbell and Travis [74], have yet been done on LX-17. So DeOliveria et al. [78] estimated values of A = 1000, ε = 0.001, a_1 = 0.50, and Fc = 0.01 to produce reasonable dead zones for the Hockey Puck corner turning experiments. For low shock pressures, these values yield desensitization times of 1.29 μs for a 1 GPa shock and 0.26 μs for a 5 GPa shock.

Using the desensitization values and the usual LX-17 Ignition and Growth parameters [76], the measured and calculated PDV axial free surface velocity histories from one of the experiments are compared in Fig. 16. The calculated jump-off times for all 40 PDV probes agree well with the experimental measurements in the five experiments. At radii greater than that of the steel plates, the LX-17 detonation waves accelerate the aluminum plates to velocities greater than 2000 m/s. At radii less than that of the steel plates, the jump-off velocities are much less lower and increase when subsequent shocks arrive.

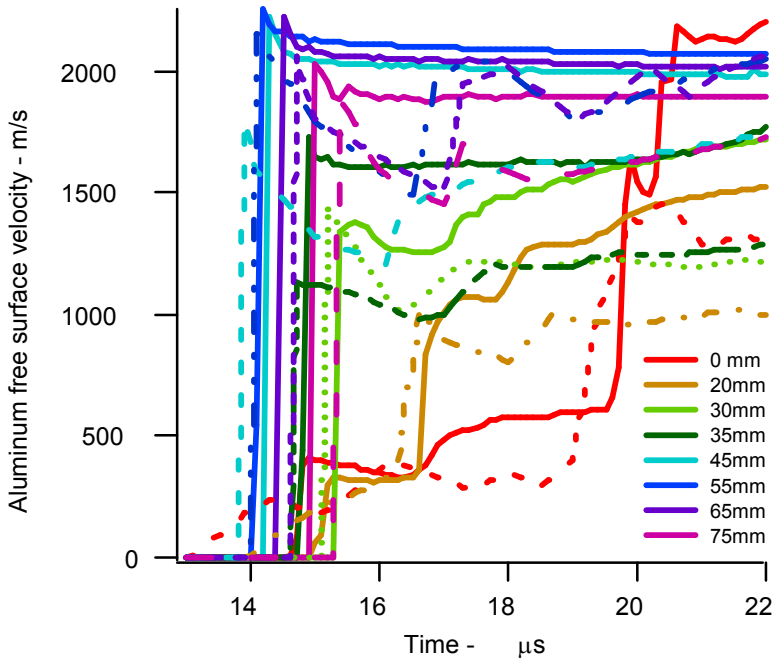

Figure 16. Measured and calculated free surface velocities for a LX-17 shock desensitization experiment

Perhaps the ultimate test of a detonation reactive flow model is a quantitative three-dimensional experiment in which the detonation wave propagates or fails to propagate. The Prism Test [17] developed by Ramsay at LANL for insensitive high explosives is the only such test. The unconfined version of this test is shown in Fig. 17. It consists of a line wave generator to initiate the top surface of a PBX 9501 (95% HMX, 2.5% BDNPA/F, and 2.5% Estane). The detonating PBX 9501 sends a detonation wave into PBX 9502, which is initially overdriven. The PBX 9502 then detonates downward in a trapazoid of decreasing thickness. At a thickness approximately equal to one half of the cylindrical failure diameter, the PBX 9502 detonation wave fails to propagate. The remaining PBX 9502 detonation wave propagates downward to an aluminum witness plate, creating a crater that clearly shows the edge of the detonation wave. Various confinement materials (water, PMMA, aluminum, copper, water, and lead) were used on the PBX 9502 boundary to change its confined failure thickness. The measured experimental failure thickness was inversely proportional to the impedance of the confinement material. Ramsay [17] studied three initial temperatures (-55˚C, 25˚C and 75˚C), and Asay and McAfee [79] fired 250˚C PBX 9502 prisms. This large experimental data set is an excellent test for three-dimensional reactive flow modeling.

Ignition and Growth model parameters for PBX 9502 [16] were determined using existing failure diameter data at -55˚C, 25˚C, 75˚C and 250 ˚C [79,80]. The only changes are B and initial temperature To in Eq. (13) and the coefficient G1 in Eq. (4). These parameters for the four temperatures are given in Table 1. The 25˚C PBX 9502 parameters were tested on previously discussed two-dimensional experiments and on the Prism test by Garcia and Tarver [18]. Recently Garcia and Tarver [81] extended the Prism Test modeling to all four initial temperatures and several confinement materials using finer three-dimensional zoning. Table 2 lists the experimental and calculated failure thicknesses for 25˚C PBX 9502 confined by various materials.

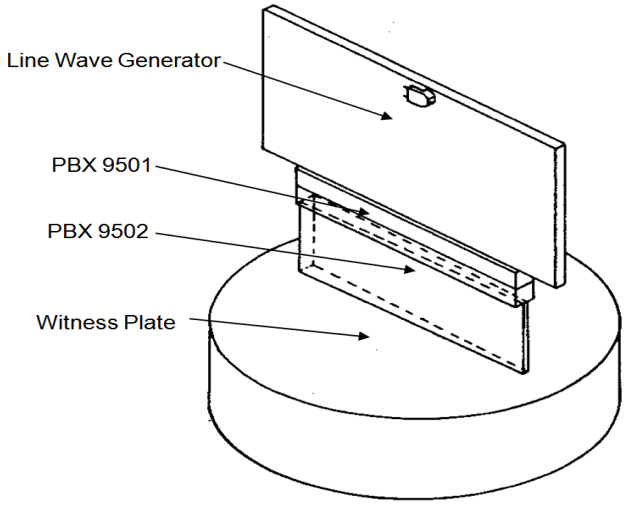

Figure 17. The unconfined LANL Prism Test geometry

Temperature (°C)	G_1 ($Mbar^{-3}\mu s^{-1}$)	B (Mbar)
-54	3750	-0.004488
25	4613	-0.05031
75	7200	-0.05376
250	8000	-0.06580

Table 1. Values of B and G_1 for various initial temperatures of PBX 9502

Material	Measured (mm)	Calculated (mm)
Unconfined	3.5	4.0
Al (0.075mm)	2.6	3.8
Al (0.5mm)	1.9	1.3
Al (1.0 mm)	1.6	<1
Steel (0.5mm)	--	<1
Copper (0.5mm)	--	<1
PMMA (1.0 mm)	3.5	2.0
PMMA (3.0 mm)	3.5	2.0

Table 2. Measured and calculated Prism failure thickness of 25˚C PBX 9502 confined by various materials

The experimental and calculated PBX 9502 unconfined failure thicknesses at the four initial temperatures are compared in Fig. 18. Considering that the -54˚C, 75˚C and 250˚C model parameters are based on only unconfined cylinder failure diameter data, the agreement with experiment is very encouraging.

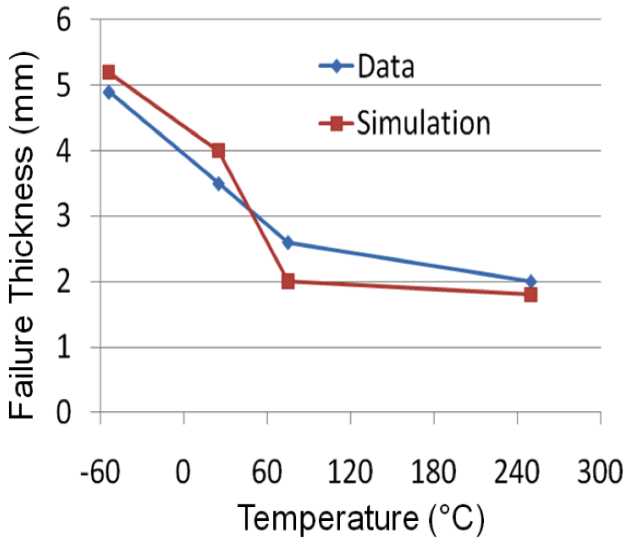

Figure 18. Experimental versus calculate PBX 9502 failure thickness for four initial temperatures

Therefore quantitative three-dimensional reactive flow modeling of condensed phase detonation waves is definitely possible given the size and speed of existing and future computers. The current calculations were done without automatic mesh refinement (AMR) techniques that make even larger scale, longer time duration calculations possible. It also appears that a set of reactive flow model parameters for a particular explosive developed using one- and two-dimensional experimental data can be reliably used for calculating three-dimensional problems. Currently, only the TATB based explosives LX-17 and PBX 9502 have been studied with all of the aforementioned experimental techniques and thus have the best developed parameter sets. HMX, RDX, TNT, and Composition B have been studied to a lesser extent [25,47,82]. Average two-dimensional reaction zone properties of detonation waves in liquid explosives, such as nitromethane, can be calculated using the Ignition and Growth model [83]. Reactive flow modeling of very "non-ideal" solid explosives, such as ammonium nitrate - fuel oil (ANFO) and aluminized explosives, is more difficult due to their extremely long reaction zone lengths and buildup distances to full C-J detonation, but it can be done.

FUTURE RESEARCH

While a great deal has been learned in recent years about the extreme chemistry occurring in a detonation reaction zone, much more research is required to fully understand the non-equilibrium processes, the reaction pathways, and the approach to equilibrium C-J mixtures created within a detonation wave. A tightly coupled experimental and theoretical approach is required to produce such an understanding. Experimental efforts are underway to measure the rates of vibrational excitation by phonon up-pumping, IVR and initial decomposition reactions. Molecular dynamics and reactive force field reaction pathway modeling is rapidly becoming more sophisticated. and larger scale systems can now be studied using parallel computers. Improved potentials are being developed to better describe partially reacted and equilibrium states.

Since chemical reaction rates and equilibrium concentrations are controlled by the local temperature in a region of molecules, the most urgent need in explosives research is for time resolved experimental measurements of temperature in all regions of reacting explosives: impact and shock induced hot spots; deflagration waves; reactive flows behind shock fronts; and detonation waves. Knowing the unreacted explosive temperature as a function of shock pressure will complete its EOS description and allow more accurate predictions of the induction time delay for the onset of bond breaking behind each individual shock front of a three-dimensional detonation wave. Accurate temperature measurements will enable molecular dynamics simulations to be done at the exact pressure, density and temperature conditions attained in various regions of a detonation wave. Temperature measurements in the vicinity of the C-J plane and in the subsequent reaction product expansion flow will eliminate the last remaining (and most important) unknown in the thermochemical equilibrium C-J predictions. Improved potentials can be developed to predict the distribution of internal and potential energies under all of the conditions attained in the flows produced by detonation waves. Then the impulse delivered to an adjoining material by a detonation wave can be more accurately modeled.

Since not all of the scenarios involving detonation waves can be tested experimentally, hydrodynamic computer models have to be improved to predict the safety and performance properties of the reactive flows produced by detonating explosives. Assuming that the necessary temperature data will soon become available, the next generation of hydrodynamic computer code reactive flow models for simulating detonation waves in one-, two-, and three-dimensions will need to be based entirely on temperature dependent Arrhenius rate laws, replacing current compression and pressure dependent rate laws. Mesoscale models are being formulated in which individual particles of a solid explosive plus their binders and voids are meshed, shocked heated, and either react or fail to react using Arrhenius kinetics. Modeling descriptions of individual particles is still impractical for larger scale simulations even with today's parallel super computers. So a continuum Statistical Hot Spot reactive flow model [84-87] is currently being developed in the ALE3D hydrodynamic computer code, which enables the complete coupling of heat transfer, chemical reactions, hydrodynamics, and chemical species equilibrium [88]. In this model, realistic numbers of hot spots of various sizes, shapes, and temperatures based on the original void volume, particle size distribution and temperature of the solid explosive are assumed to be created as the initiating shock front compresses the explosive particles. The hot spots then either react and grow into the surrounding explosive or fail to react and die out based on multistep Arrhenius kinetics rates. The Statistical Hot Spot reactive flow model accurately simulates shock desensitization without a separate desensitization rate law. The coalescence of growing hot spots at high pressures and temperatures, the creation of additional surface area available to the reacting sites as the pressure rises, the rapid transition to detonation, and the formation of the three-dimensional cellular structure of self-sustaining detonation are four of the most challenging current problems under investigation in hydrodynamic reactive flow modeling efforts on homogeneous and heterogeneous condensed phase explosives.

ACKNOWLEDGMENTS

It is impossible to individually thank all of the great experimentalists and theoreticians who developed the current understanding of condensed phase detonation over the past forty years. The author thanks them all collectively for their hard word and enthusiasm. This work was performed under the auspices of the U.S. Department of Energy by the Lawrence Livermore National Laboratory under Contract DE-AC52-07NA27344.

REFERENCES

1. W. Fickett and W. C. Davis, *Detonation Theory and Experiment*, Dover Publications, Mineola, NY, 2000.

2. W. Fickett, *Introduction to Detonation Theory*, University of California Press, Berkeley, CA, 1984.

3. A. N. Dremin, *Toward Detonation Theory*, Springer-Verlag, New York, 1999.

4. C. M. Tarver, "What is a Shock Wave to an Explosive Molecule?" *High-Pressure Shock Compression of Solids VI*, Y. Horie, L. Davidson, and N. N. Thadhani, eds., Springer-Verlag, New York, 2003, p. 323.

5. M. R. Manaa, ed., *Chemistry at Extreme Conditions*, Elsevier, Amsterdam, 2005.

6. B. Dobratz, *Detonation and Combustion of Explosives: A Selected Bibliography*, Eleventh International Detonation Symposium, Office of Naval Research ONR 33300-5, Snoqmass, CO, 1998, p. 1101.

7. B. W. Asay, J. E. Kennedy, J. B. Ramsay, F. J. Schelling, and B. E. Takala, *Indices of the Proceedings for the Thirteen International Symposia on Detonation 1951 - 2006*, Los Alamos National Laboratory Report LA-UR-07-4550, 2007.

8. J. H. S. Lee, *The Detonation Phenomenon*, Cambridge University Press, Cambridge, 2008.

9. I. Plaksin, C. S. Coffey, R. Mendes, J. Riberio, J. Campos, and J. Direito, *Thirteenth International Detonation Symposium*, Office of Naval Research ONR 351-07-01, Norfolk, VA, 2006, p. 319.

10. B. Hayes and C. M. Tarver, *Seventh Symposium (International) on Detonation*, Naval Surface Weapons Center NSWC MP 82-334, Annapolis, MD, 1981, p. 1029.

11. S. A. Sheffield, R. Engelke, R. R. Alcon, R. L. Gustavsen, D. L. Robbins, D. B. Stahl. H. L. Stacy, and M. C. Whitehead, *Twelfth International Detonation Symposium*, Office of Naval Research ONR 333-05-2, San Diego, CA, 2002, p. 159.

12. A. P. Ershov, N. P. Satonkina, and G. M. Ivanov, *Thirteenth International Detonation Symposium*, Office of Naval Research ONR 351-07-01, Norfolk, VA, 2006, p. 79.

13. C. M. Tarver, J. W. Kury, and R. D. Breithaupt, *J. Appl. Phys*. **82**, 3771 (1997).

14. Y. Kato, N. Mori, H. Sakai, K. Tanaka, T. Sakurai, and T. Hikita, *Eighth Symposium (International) on Detonation*, Naval Surface Weapons Center NSWC MP 86-194, Albuquerque, NM, 1985, p. 558.

15. S. Bastea, K. R. Glaesemann, and L. E. Fried, *Thirteenth International Detonation Symposium*, Office of Naval Research ONR 351-07-01, Norfolk, VA, 2006, p. 1137.

16. C. M. Tarver and E. M. McGuire, *Twelfth International Detonation Symposium*, Office of Naval

Research ONR 333-05-2, San Diego, CA, 2002, p. 641.

17. J. B. Ramsay, *Eighth Symposium (International) on Detonation*, Naval Surface Weapons Center NSWC MP 86-194, Albuquerque, NM, 1985, p. 372.

18. M. L. Garcia and C. M. Tarver, *Thirteenth International Detonation Symposium*, Office of Naval Research ONR 351-07-01, Norfolk, VA, 2006, p. 63.

19. C. M. Tarver, *Combustion and Flame* **46**, 111, 135, 157 (1982).

20. C. M. Tarver, L. E. Fried, A. J. Ruggerio, and D. F. Calef, *Tenth International Detonation Symposium*, Office of Naval Research ONR 33395-12, Boston, MA, 1993, p. 3.

21. C. M. Tarver, *Shock Compression of Condensed Matter-1997*, AIP Conference Proceedings 429, 1998, Amherst, MA, p. 301.

22. C. M. Tarver, *J. Phys. Chem. A* **101**, 4845 (1997).

23. C. M. Tarver, *Shock Compression of Condensed Matter - 1999*, AIP Conference Proceedings 505, 2000, Snowbird, UT, p. 873.

24. C. M. Tarver, *Shock Compression of Condensed Matter - 2001*, AIP Conference Proceedings 620, 2002, Atlanta, GA, p. 42.

25. C. M. Tarver, *Shock Compression of Condensed Matter - 2005*, AIP Conference Proceedings 845, Baltimore, MD, 2005, p.1026.

26. D. L. Chapman, *Phil. Mag*. **213**, Series 5, 47, 90 (1899).

27. E. Jouguet, *Pure Appl. Math.* **70**, Series 6, 1, 347 (1904)

28. Y. B. Zeldovich, *J. Exper. Theor. Phys. (USSR)* **10**, 542 (1940).

29. J. Von Neumann, *Office of Science Research and Development Report No. 549* (1942).

30. W. Doring, *Am. Physik* **43**, 421 (1943).

31. W. W. Wood and J. G. Kirkwood, *J. Chem. Phys*. **29**, 957 (1958).

32. C. M. Tarver, J. O. Hallquist, and L. M. Erickson, *Eighth Symposium (International) on Detonation*, Naval Surface Weapons Center NSWC MP 86-194, Albuquerque, NM, 1985, p. 951.

33. Y. B. Zel'dovich and Y. P. Raizer, *Physics of Shock waves and High-Temperature Hydrodynamic Phenomena*, Academic Press, NY, 1966.

34. R. E. Weston, Jr. and G. W. Flynn, *Ann. Rev. Phys. Chem*. **43**, 559 (1993).

35. X. Hong, S. Chen, and D. D. Dlott, *J. Phys. Chem*. **99**, 9102 (1995).

36. W. Holmes, W., R. S. Francis, and M. D. Fayer, *J. Chem. Phys*. **110**, 3576 (1999).

37. J. Hopper, "On the Role of Phonon Scattering Processes in Shock-induced Initiation," *Fourteenth International Detonation Symposium*, Coeur d'Alene, ID, April 2010, in press.

38. E. J. Reed, M. R, Manaa, L. E. Fried, K. R. Glaesemann, C. M. Tarver, and J. D. Joannopoulos, "Ab-initio Discovery of Ultrafast Detonation, Metallization and Chapman-Jouguet States in Nitromethane and Hydrozoic Acid," *Fourteenth International Detonation Symposium*, Coeur d'Alene, ID, April 2010, in press.

39. L. G. Green, C. M. Tarver, and D. J. Erskine, *Ninth Symposium (International) on Detonation*, Office of the Chief of Naval Research OCNR 113291-7, Portland, OR, 1989, p. 670.

40. J. H. Kiefer and S. S. Kumaram, *J. Chem. Phys*. **99**, 3531 (1993).

41. H. Eyring, *Science* **199**, 740 (1978).

42. V. Bernshtein and I. Oref, *J. Phys. Chem*. **100**, 9738 (1996).

43. J. H. L. Lee, "On the Universal Role of Turbulence in the Propagation of Strong Shocks and Detonation Waves," *High-Pressure Shock Compression of Solids VI*, Y. Horie, L. Davidson, and N. N. Thadhani, ed., Springer-Verlag, New York, 2003, p. 121.

44. A. A. Vasil'ev and A. V. Trotsyuk, *Combustion, Explosion and Shock Waves* **39**, 80 (2003).

45. V. N. Gamezo, D. Desbordes, and E. S. Oran, *Shock Waves* **9**, 11 (1999).

46. J. A. Viercelli and J. N. Goeski, *J. Chem. Phys*. **117**, 11352 (2002).

47. J. W. Kury, R. D. Breithaupt, and C. M. Tarver, *Shock Waves* **9**, 227 (1999).

48. W. C. Tao, C. M. Tarver, J. W. Kury, C. G. Lee, and D. L. Ornellas, *Tenth International Detonation Symposium*, Office of Naval Research ONR 33395-12, Boston, MA, 1993, p. 628.

49. L. I. Stiel, E. L. Baker, and C. Capellos, "Characteristic Melt Times and Onset of Reaction for Aluminized Explosives," *Fourteenth International Detonation Symposium*, Coeur d'Alene, ID, April 2010, in press.

50. A. L. Kuhl, H. Reichenbach, J. B. Bell, and V. E. Beckner, "Reactive Blast Waves from Composite Charges," *Fourteenth International Detonation Symposium*, Coeur d'Alene, ID, April 2010, in press.

51. D. L. Frost, S. Goroshin, R. Ripley, and F. Zhang, "Interaction of a Blast Wave with a Metalized Explosive Fireball," *Fourteenth International Detonation Symposium*, Coeur d'Alene, ID, April 2010, in press.

52. W. L. Seitz, H. L. Stacy, R. Engelke, P. K. Tang, and J. Wackerle, *Ninth Symposium (International) on Detonation*, Office of the Chief of Naval Research OCNR 113291-7, Portland, OR, 1989, p. 657.

53. N. V. Kozyrev, B. V. Larinov, and G. V. Sakovich, *Combustion, Explosion and Shock Waves* **44**, 193 (2008).

54. C. M. Tarver, N. L. Parker, H. G. Palmer, B. Hayes, and L. M. Erickson, *J. Energetic Materials* **1**, 213 (1983).

55. S. A. Sheffield, D. D. Bloomquist, and C. M. Tarver, *J. Chem. Phys.* **80**, 3831 (1984).

56. M. M. Gorshkov, K. F. Grebenkin, V. M. Slobodenyukov, O. V. Tkachev, V. T. Zaikin, and A. L. Zherebtsov, *Thirteenth International Detonation Symposium*, Office of Naval Research ONR 351-07-01, Norfolk, VA, 2006, p. 435.

57. P. A. Urtiew and C. M. Tarver, *Combustion, Explosion, and Shock Waves* **41**, 766 (2005).

58. P. A. Urtiew, K. S. Vandersall, C. M. Tarver, F. Garcia, and J. W. Forbes, *Thirteenth International Detonation Symposium*, Office of Naval Research ONR 351-07-01, Norfolk, VA, 2006, p. 929.

59. K. S. Vandersall, C. M. Tarver, F. Garcia, and S. K. Chidester, *J. Appl. Phys*. **107**, 094906 (2010).

60. C. M. Tarver, *Propellants, Explosives, Pyrotechnics* **15**, 132 (1990).

61. C. M. Tarver and P. A. Urtiew, *Progress in Astronautics and Aeronautics* **94**, 369 (1985).

62. C. M. Tarver, W. C. Tao, and C. G. Lee, *Propellants, Explosives, Pyrotechnics* **21**, 238 (1996).

63. C. M. Tarver, R. D. Breithaupt, and J. W. Kury, *J. Appl. Phys*. **81**, 7193 (1997).

64. A. W. Campbell and R. Engelke, *Sixth Symposium (International) on Detonation*, Office of Naval Research ACR-221, Coronado, CA, 1976, p. 642.

65. G. A. Leiper and J. Cooper, *Ninth Symposium (International) on Detonation*, Office of the Chief of Naval Research OCNR 113291-7, Portland, OR, 1989, p. 197.

66. C. L. Mader, *Sixth Symposium (International) on Detonation*, Office of Naval Research ACR-221, Coronado, CA, 1976, p. 405.

67. E. N. Ferm, C. L. Morris, J. P. Quintana, P. Pazuchanic, H. Stacy, J. D. Zumbro, G. Hogan, and N. King, *Shock Compression of Condensed Matter - 2001*, AIP Conference Proceedings 620, Atlanta, GA, 2002, p. 966.

68. R. L. Druce, F. Roeske, P. C. Souers, C. M. Tarver, C. T. S. Chow, R. S. Lee, E. M. McGuire, G. E. Overturf, and P. A. Vitello, *Twelfth International Detonation Symposium*, Office of Naval Research ONR 333-05-2, San Diego, CA, 2002, p. 675.

69. C. M. Tarver, *Propellants, Explosives, Pyrotechnics* **30**, 109 (2005).

70. C. M. Tarver and S. K. Chidester, *Shock Compression of Condensed Matter-2009*, AIP Conference Proceedings 1195, Nashville, TN, 2009, p. 249.

71. S. N. Lubyatinsky, S. V. Batalov, A. Y. Garmashev, V. G. Israelyan, O. V. Kostitsyn, B. G. Loboiko. V. A. Pashentsev, E. B. Smirnov, and V. P. Filin, *Shock Compression of Condensed Matter - 2003*, AIP Conference Proceedings 706, Portland, OR, 2003, p. 859.

72. T. L. Salyer and L. G. Hill, *Thirteenth International Detonation Symposium*, Office of Naval Research ONR 351-07-01, Norfolk, VA, 2006, p. 24.

73. F. P. Bowden and A. D. Yofee, *Ignition and Growth of Explosion in Liquids and Solids*, Cambridge University Press, Cambridge, UK, 1985.

74. A. W. Campbell and J. R. Travis, *Eighth Symposium (International) on Detonation*, Naval Surface Weapons Center NSWC MP 86-194, Albuquerque, NM, 1985, p. 1057.

75. M. R. Hart, "Jack Rabbit Investigation of TATB IHE Detonation Chemical Kinetics," *Fourteenth International Detonation Symposium*, Coeur d'Alene, ID, April 2010, in press.

76. C. M. Tarver, *J. Phys. Chem. A* **114,** 2727 (2010).

77. C. M. Tarver, T. M. Cook, P. A. Urtiew, and W. C. Tao, *Tenth International Detonation Symposium*, Office of Naval Research ONR 33395-12, Boston, MA, 1993, p. 696.

78. G. DeOliveira, A. K. Kapila, D. W. Schwendeman, J. B. Bdzil, W. D. Henshaw, and C. M. Tarver, *Thirteenth International Detonation Symposium*, Office of Naval Research ONR 351-07-01, Norfolk, VA, 2006, p. 13.

79. B. W. Asay and J. M. McAfee, *Tenth International Detonation Symposium*, Office of Naval Research ONR 33395-12, Boston, MA, 1993, p. 485.

80. A. W. Campbell, *Propellants, Explosives, Pyrotechnics* **9**, 183 (1984).

81. M. L. Garcia and C. M. Tarver, "Three-Dimensional Ignition and Growth Reactive Flow Modelling of Confined and Hot Prism Tests," *Fourteenth International Detonation Symposium*, Coeur d'Alene, ID, April 2010, in press.

82. P. A. Urtiew, K. S. Vandersall, C. M. Tarver, F. Garcia, and J. W. Forbes, *Thirteenth International Detonation Symposium*, Office of Naval Research ONR 351-07-01, Norfolk, VA, 2006, p. 929.

83. C. M. Tarver and P. A. Urtiew, "Theory and Modelling of Liquid Explosive Detonation," *J. Energetic Materials*, 2010, in press.

84. A. L. Nichols III and C. M. Tarver, *Twelfth International Detonation Symposium*, Office of Naval Research ONR 333-05-2, San Diego, CA, 2002, p. 489.

85. A. L. Nichols III, C. M. Tarver, and E. M. McGuire, *Shock Compression of Condensed Matter -2003*, AIP Conference Proceedings 706, Portland, OR, 2003, p. 397.

86. A. L. Nichols III, *Shock Compression of Condensed Matter - 2005*, AIP Conference Proceedings 845, Baltimore, MD, 2005, p. 465.

87. A. L. Nichols III, "Comparison of the Growth of Pore and Shear Band Driven Detonations," *Fourteenth International Detonation Symposium*, Coeur d'Alene, ID, April 2010, in press.

88. A. L. Nichols III, ed. "User's Manual for ALE3D, an Arbitrary Lagrange/Eulerian 2D and 3D Code System," *Lawrence Livermore National Laboratory Report LLNL-SM-404490 Rev. 1*, 2009.